PAPER • OPEN ACCESS

Half-wavelength velocity bunching: non-adiabatic temporal focusing of charged particle beams

To cite this article: Anatoliy Opanasenko *et al* 2023 *New J. Phys.* **25** 123049

IOP Publishing New J. Phys. 25 (2023) 123049 https://doi.org/10.1088/1367-2630/ad1717

New Journal of Physics
The open access journal at the forefront of physics

Deutsche Physikalische Gesellschaft DPG
IOP Institute of Physics

Published in partnership with: Deutsche Physikalische Gesellschaft and the Institute of Physics

OPEN ACCESS

RECEIVED
27 September 2023

REVISED
7 December 2023

ACCEPTED FOR PUBLICATION
19 December 2023

PUBLISHED
29 December 2023

PAPER

Half-wavelength velocity bunching: non-adiabatic temporal focusing of charged particle beams

Anatoliy Opanasenko[1], **Giovanni Perosa, Johan Ribbing and Vitaliy Goryashko**[*]

FREIA Laboratory, Uppsala University, Uppsala, Sweden
[1] Also at National Science Center 'Kharkiv Institute Physics and Technology', Kharkiv, Ukraine.
[*] Author to whom any correspondence should be addressed.

E-mail: vitaliy.goryashko@physics.uu.se

Keywords: femtosecond high-brightness electron beams, space-charge, bunch compression

Supplementary material for this article is available online

Abstract

X-ray free-electron lasers (XFELs) and megaelectronvolt ultrafast electron diffractometers (MeV UEDs) are revolutionary scientific instruments that allow visualizing the dynamics of elementary excitations in a wide range of systems from atoms and molecules to phonons, magnons and plasmons. Femtosecond (fs) electron beams are at the heart of XFELs and MeV UEDs, and the formation of fs electron beams with ultrahigh brightness is the subject of active research. We report an interesting regime of non-adiabatic temporal compression of electron beams by two orders of magnitude. Via analytical calculations and numerical simulations, we show that few MeV electron bunches can be trapped and compressed by a strong electromagnetic field within a half of the field wavelength. Furthermore, in a multi-cell accelerating cavity, the bunch is first compressed and then accelerated, thus allowing one to preserve very short bunch duration. For example, a 3 ps 16 pC 1 MeV electron bunch is compressed to 21 fs rms and accelerated to 12 MeV in a TESLA superconducting cavity. Another example is the production of 1.2 fs 16 fC 3.3 MeV bunches with a coherence length of 20 nm and and an energy spread less than 3 keV. The discovered mechanism of compression, which is another mode of velocity bunching, opens the door for obtaining very high electron brightness.

1. Introduction

Brightness is a figure-of-merit for beam quality, representing the charged beam phase space density [1]. The interest in high-brightness electron sources unites many accelerator-based applications, from x-ray free-electron lasers, plasma wakefield acceleration and inverse-Compton scattering to colliders, ultrafast electron microscopes and diffractometers [2–11]. The concept of megaelectronvolt ultrafast electron diffraction (MeV UED), proposed in [12] and successfully demonstrated experimentally in [6, 13], has resulted in the establishment of a discovery-rich user facility at the Stanford National Accelerator Laboratory [10]. Currently, MeV UEDs operate with 100 fs resolution demonstrated in [10, 13, 14] but simulation results in [14] indicate that a 5 fC 2.8 MeV electron bunch could be as short as 10 fs rms. However, we shall see in this manuscript that a bunch duration of even 1.2 fs rms can be reached.

High brightness is achieved in systems able to deliver low emittance, high peak current and ultrashort duration electron beams. For this reason, the temporal focusing of charged beams, referred as longitudinal compression or bunching, became a staple for designing high-brightness electron sources. In its most basic form, bunching is achieved by imprinting an energy-position correlation (called also *energy chirp*) into the electron bunch. The electrons in the bunch tail are made to have a higher energy than those in the head. Then, the fast electrons catch up with the slow ones as the bunch propagates, for example, in free space leading to bunch compression. This basic mechanism of compression, known as ballistic bunching, was discovered almost a century ago [15] but still of interest and used in electron sources [16]. It is very efficient if applied to uniformly filled ellipsoidal bunches or bunches with very low charges [17–19].

In general, however, the ballistic bunching process is accompanied by degradation of the beam quality in the transverse phase space because of nonlinear Coulomb forces [20]. Thus, several other bunching techniques have been developed, in particular, for high-energy beams [21]. In this paper, we focus on the compression of low-energy beams as a pre-requisite for compact FELs, laser-based Compton sources and UEDs [22].

To address the problem of emittance degradation during ballistic bunching in free space or magnetic bunching in a chicane, the concept of velocity bunching was introduced [23]. This approach combines bunching with acceleration, thereby preserving the quality of the bunch [24–27]. It is worth noting that the effect of velocity bunching was initially proposed and experimentally demonstrated in the study by Wang *et al* [24].

The method of velocity bunching is widely used nowadays and adopted, for example, at the SACLA FEL [28]. A moderate compression factor of around 10–20 (the reduction of the bunch length) is, however, a limitation of velocity bunching [24].

In this work, we demonstrate the possibility to achieve a highly efficient *non-adiabatic* compression of electron beams, capable of reducing the bunch length by more than *two orders of magnitude*[2]. Longitudinal focusing occurs on a very short length scale, corresponding to a half of the wavelength of the field used for compression. For this reason, we name it half-wavelength bunching (HWB). To our knowledge, this phenomenon has never been demonstrated before.

In contrast, in the schemes of ballistic and velocity bunching, the duration of the bunch compression process is long compared to the characteristic time-scale of the field used for compression. For this reason we refer to them as adiabatic compression schemes.

Our scheme has distinct features: (1) very short compression length: bunching occurs within a half of the wavelength of the field; (2) very strong compression: the bunch length can be reduced by more than two orders of magnitude for parameters achievable in practice; (3) compression and acceleration are performed in the same structure, making the whole system compact; (4) in contrast to ballistic bunching, there is no phase jitter between the fields used for compression and further acceleration; (5) our compression scheme is quite immune to the amplitude and phase jitter of the electromagnetic field used for compression.

Our scheme is best suited for few MeV beams if traditional accelerator technology is used. The energy gain over a quarter of the wavelength of the field used for compression must be approximately equal to the beam energy at injection. This places a limitation either on the beam energy or the applied accelerating field. A typical optimum regime corresponds to a peak accelerating *field* of 30 MV m^{-1} for a 1 MeV beam.

2. Concept

To illustrate the concept of HWB, we refer to figure 1, which shows the evolution of the longitudinal phase space (z, p_z) of a realistic electron bunch in a 1-cell elliptical 1.3 GHz cavity. Here z is the coordinate normalised to the radiofrequency (RF) field wavelength λ.

The low energy of the electron beam upon the injection into the cavity, together with its strong *field* of 30 MV m^{-1}, allows for an unusual regime of bunching. The bunch is injected into a decelerating phase of -60^o w.r.t. the zero crossing of the *standing wave field* (dark blue region). Note that this choice of the time-zero phase corresponds to the maximum energy gain in a standing wave with a sin-like dependence on time, see the right plot in figure 1. Simultaneously, the bunch acquires an energy chirp needed for compression while its energy is dramatically reduced down to around 200 keV. Thanks to this extreme low bunch energy and the large energy chirp acquired earlier, the longitudinal focusing length is just a few cm corresponding to a quarter of the wavelength. After passing the decelerating field phase, the bunch slips further into an accelerating phase (red shaded area) and recovers its energy, thus having Coulomb repulsion suppressed through the relativistic effect.

Figure 1 also shows the variation of the ratio of the current bunch length to the initial one along the cavity, which is the inverse compression factor η. The abrupt variation in the bunch length is localised around the cavity center. Differently from velocity bunching, the bunch motion is not synchronous with the RF field propagation.

It worth mentioning that numerical simulations performed in [18] showed that significant deceleration in the first cell enhances the compression of electron bunches. However, the compression effect in the first cell was a factor of 3 and the study [18] did not receive a further attention.

[2] After this study was completed, the authors got to know that the enhancement of bunch compression via substantial deceleration was already noticed in numerical simulations of [18]. However, the physics of the effect was not investigated and largely remained unknown in the literature.

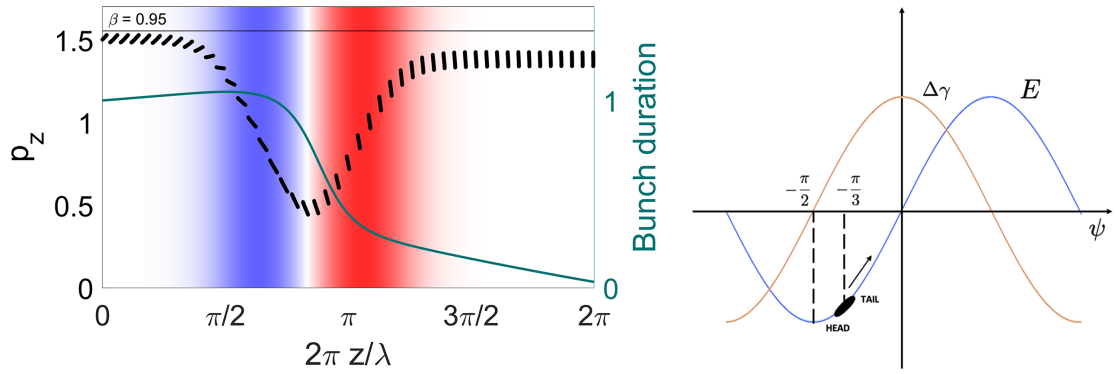

Figure 1. Left: Longitudinal phase space of the electron bunch (black) is shown at different positions along a 1-cell 1.3 GHz cavity. The shaded color map represents the instantaneous electric field in the cavity acting on the electrons. The red and blue regions correspond to the accelerating and decelerating field phases. The green line shows the ratio of the current bunch length to the initial one. The results are based on simulations performed with the code ASTRA [29] and employ a realistic bunch distribution from a photo-injector described in [30]. The initial bunch energy is 1 MeV. The momentum corresponding to $\beta = 0.95$ is shown as a reference. Right: phase convention in this study. $E(\psi)$ is the dependence of the electric field on the phase, and $\Delta\gamma$ is the energy gain vs phase for a relativistic test electron in a weak accelerating field.

Now, we will introduce a 1D-model that captures all essential physics of the HWB process. We consider the motion of electrons along the symmetry axis of the cavity

$$\frac{d\psi}{d\zeta} = \frac{\gamma}{\sqrt{\gamma^2 - 1}}, \quad \frac{d\gamma}{d\zeta} = \frac{eE_z(\zeta)}{mc^2} = \alpha g(\zeta)\sin(\psi), \tag{1}$$

where $k = 2\pi/\lambda$ is the wave vector in free space, $\alpha = eE_0/kmc^2$ is the effective energy gain normalised to the rest mass mc^2 and E_0 is the peak accelerating *field*. The phase ψ and the relativistic factor γ are functions of the longitudinal coordinate $\zeta = kz$. The inverse compression factor η satisfies the equation (see appendix for details)

$$\frac{d^2\eta}{d\zeta^2} + 3\gamma_r \frac{\alpha g(\zeta)\sin(\psi_r)}{\gamma_r{}^2 - 1}\frac{d\eta}{d\zeta} + \frac{\alpha g(\zeta)\cos(\psi_r)}{(\gamma_r{}^2 - 1)^{\frac{3}{2}}}\eta = 0 \tag{2}$$

with initial conditions: $\eta(\zeta_0) = 1$, $\eta'(\zeta_0) = -\partial\beta_0/\partial\psi_0/\beta_0^2$. Here, γ_r and ψ_r are the energy and phase of the reference particle governed by the equation (1). Equations (1) and (2) constitute a useful simulation tool that allows quickly and accurately compare different regimes of bunching without time-consuming particle tracking.

The evolution of the longitudinal phase-space bunch distribution, obtained with this simple model, is in a very good agreement with that obtained from 3D space-charge dominated dynamics simulated with the code ASTRA [29].

A numerical solution to the model (1) is shown in figure 2. An initial ensemble of electrons is represented by five distributions corresponding to five discrete energy levels. In the figure, these distributions are marked by colored dots having five different starting values of the longitudinal momentum p_z. Each distribution is composed of 500 particles with initial injection phases linearly distributed between 0 and 2π. In the configuration spaces, these particles are distributed between between 0 and λ and the color coding is used to distinguish them.

The highest momentum particles are not significantly bunched within the extent of the cavity. These will undergo ballistic compression in free space after the cavity. The particles with the lowest momentum are reflected by the cavity field and move in the backward direction.

The strongly bunched particles (same longitudinal positions) are the ones having the initial momentum slightly above the critical value corresponding to the reflection from the cavity. Furthermore, there is a region of initial phases that corresponds to strong compression with a large final negative momentum chirp, which can compensate for Coulomb repulsion.

Let us examine the process of HWB and try to capture the scaling of the parameters leading to bunching. We introduce a 3-step model visualized in figure 1:

- step 1: deceleration and energy chirp accumulation;
- step 2: field-free bunch rotation in the phase space and transition to the accelerating phase;
- step 3: acceleration and velocity bunching.

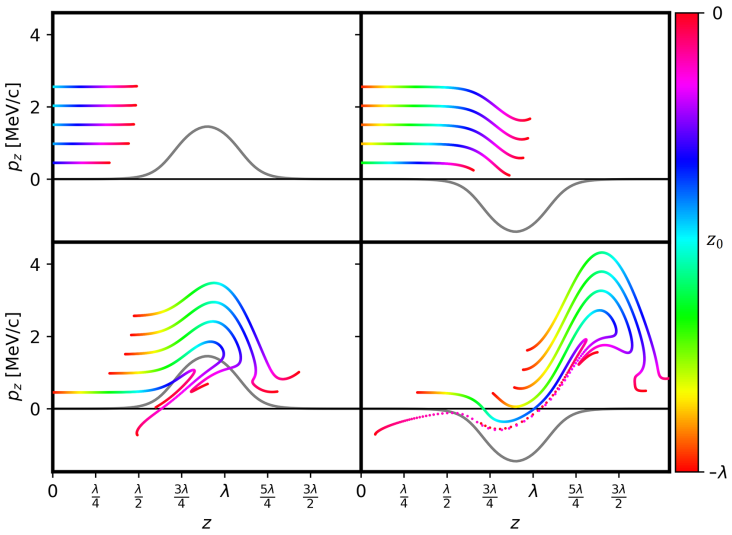

Figure 2. Snapshots of phase space for 1D non-interacting model (1) in a single cell cavity. The color of phase space points indicate starting z_0 value and the black solid line is the instantaneous electric field, scaled for visual convenience. An animation is available in the Supplementary materials.

There is no sharp transition between different steps but since our goal to obtain simple order-of-magnitude estimates, the 3-step model is good enough.

Step 1: in the physical space, the deceleration occurs over the distance of $\lambda/4$, which corresponds to $\Delta\zeta = \pi/2$. Then, the energy loss can be estimated as

$$\Delta\gamma \sim (\pi/2)\,\alpha\bar{g}\sin(\psi_0)\,. \tag{3}$$

Neglecting the initial energy chirp, the acquired chirp along the bunch is estimated as $\partial\gamma/\partial\psi_0$ and reads

$$\partial\gamma/\partial\psi_0 \sim (\pi/2)\,\alpha\bar{g}\cos(\psi_0)\,. \tag{4}$$

Obviously, the conditions of the maximum deceleration and maximum energy chirp are conflicting, and a possible *trade-off* is to choose $\psi_0 = -\pi/4$. Note the minus sign that corresponds to deceleration.

Step 2: the next requirement is that the bunch rotates in the phase space and takes on the upright position corresponding to bunching. The condition for the beam with a linear energy chirp to bunch over $\lambda/4$ in a field-free region is

$$kz_{\rm opt} = \frac{\beta_m^2}{\partial\beta/\partial\psi_0} = \pi/2, \tag{5}$$

where β is the longitudinal velocity normalized to the speed of light and β_m is some minimum velocity. A brief derivation of equation (5) is as follows: let an electron have a velocity modulation $v(\psi_0)$, which was acquired in a cavity field with a phase $\psi_0 = \omega t_0$. Here, the time moment t_0 is the injection time into the cavity. Now, suppose that the velocity-modulated electrons propagate in free space after the modulating cavity ($z > 0$). The arrival time of the electrons to a longitudinal position z is given by

$$t_{\rm e} = t_0 + \int_0^z \frac{dz}{v(\psi_0)} = t_0 + \frac{z}{v(\psi_0)}.$$

The requirement having the beam bunched means that all electrons arrive simultaneously at some longitudinal position, which implies $\partial t_{\rm e}/\partial t_0 = 0$. The latter condition leads to

$$1 = \frac{z}{v}\frac{\partial v/\partial t_0}{v} \;\rightarrow 1 = \frac{kz}{\beta^2}\frac{\partial\beta}{\partial\psi_0}.$$

Step 3: once the bunch rotated in the phase space, it is advantageous to accelerate it back to the initial energy to suppress Coulomb expulsion through the relativistic effect. To this end, we impose a condition that

the phase slippage over $\Delta\zeta = \pi/2$ does not exceed π so that the bunch does not slip into the decelerating phase again, i.e. $(d\psi/d\zeta)\,\Delta\zeta < \pi$,

$$(\pi/2)\,\gamma_m/\sqrt{\gamma_m^2 - 1} < \pi, \quad \gamma_m > \sqrt{4/3}. \tag{6}$$

Hence, there is a limit on how much the bunch can be decelerated in order to not be trapped by the field.

Now, we use the estimate (6) to work out a solution for α and ψ_0. The velocity chirp can be expressed as $\partial\beta/\partial\psi_0 = 1/(\beta\gamma^3)\partial\gamma/\partial\psi_0$, where the last term is given by equation (4). Then, from equations (3) and (4) we obtain

$$\alpha = \frac{4}{\pi^2}\frac{\beta_m^3\gamma_m^3}{\bar{g}\cos\psi_0} = \frac{0.73}{\bar{g}\cos\psi_0}, \quad \gamma_0 = \gamma_m - \frac{\pi}{2}\alpha\bar{g}\sin\psi_0. \tag{7}$$

Numerical simulations suggest that $\bar{g} \approx 1$ for a 1-cell cavity. Then, the optimum initial phase is estimated as

$$\psi_0 = \arctan\left[\frac{\pi}{2}\frac{\gamma_m - \gamma_0}{\beta_m^3\gamma_m^3}\right] \approx \arctan\left[0.87\,(1.15 - \gamma_0)\right]. \tag{8}$$

For an initial beam energy of 1.1 MeV, the optimum injection phase and normalized field amplitude are $\psi_0 \approx -\pi/3$ and $\alpha \approx 1.5$. This result differs only by 10% from the result of full 3D simulations with ASTRA. Equations (7) and (8) give a good starting point for 3D space-charge particle tracking.

3. Multi-stage compression in a superconducting TESLA cavity

Let us demonstrate how HWB can be combined with velocity bunching to reach bunch compression by more than two orders of magnitude and simultaneously accelerate the bunch to 'freeze' the resulting distribution through the relativistic effect[3]. We consider a realistic electron bunch distribution [30] with 16 pC of the total charge, mean energy 1.1 MeV, 3 ps rms duration, 0.08 μm emittance and 10 keV energy spread [30]. We use the simulation code ASTRA to track the bunch through a superconducting TESLA cavity [31] operated at 1.3 GHz.

Figure 3 shows a scan of the output bunch parameters over the accelerating gradient of the cavity and the injection phase, which is the field phase 'seen' by the bunch when it enters the cavity. In the rest of the text, the accelerating gradient is used to specify the cavity settings as it is common in accelerator engineering. For the TESLA cavity, an on-axis peak accelerating field of 1 MV m^{-1} corresponds to an average gradient of 0.36 MV m^{-1} for the transit-time factor of unity.

The compression factor (top left plot) in figure 3 reaches the values over 100 in a broad range of the field parameters. In particular, there is quite a broad optimum region corresponding to the gradient of 10.8 MV m^{-1} (peak on-axis field of 30 MV m^{-1}) and the injection phase of around -66°. The phase is measured from the *zero-crossing of the field* of the standing wave and the minus sign points corresponds to deceleration. For low fields, the zero phase corresponds to the maximum energy gain in the first cavity cell. If the field is too strong and the bunch is injected into the maximum deceleration phase, then the electrons are reflected back by the field, which is manifested through the white regions in the plots. What is interesting and even unexpected is that the maximum compression corresponds to the minimum energy spread and low emittance. The energy chirp (correlated energy spread) is transferred to the potential energy of the Coulomb field—a known but rarely reached regime [18].

Figure 4 gives an insight into the bunch evolution along the cavity in the regime of optimum compression. Note a unique situation: a triple compression in the cavity. Two stages of HWB in the first two cells are followed by classical velocity bunching, which allows compressing the bunch down to 21 fs rms. The transverse emittance is large but mostly correlated and can be compensated for downstream the accelerator. The longitudinal emittance is reduced by a factor of 4.

The mechanism of emittance growth observed in figure 4 is twofold: (1) a growth of slice emittance through a nonlinear deformation of the phase space and (2) an increase in projected emittance because of the misalignment of slices in the phase space. By applying a focusing magnetic field both contributions to the emittance growth can be reduced. The effect of emittance compensation is demonstrated in figure 5, where a solenoid is added after a TESLA cavity. At this high beam energy of 10 MeV, one would use a focusing triplet in practice but the solenoid suffices to demonstrate the physics. The cavity phase is tuned to -65.25° in order to move the longitudinal focus to the position of around 3.5 m if no transverse focusing is present. With the transverse focusing by a 0.6 T solenoid acting on the bunch, the space-charge density starts to

[3] The transverse space-charge force is reduced by a factor γ^2 whereas the longitudinal one by a factor of γ^3.

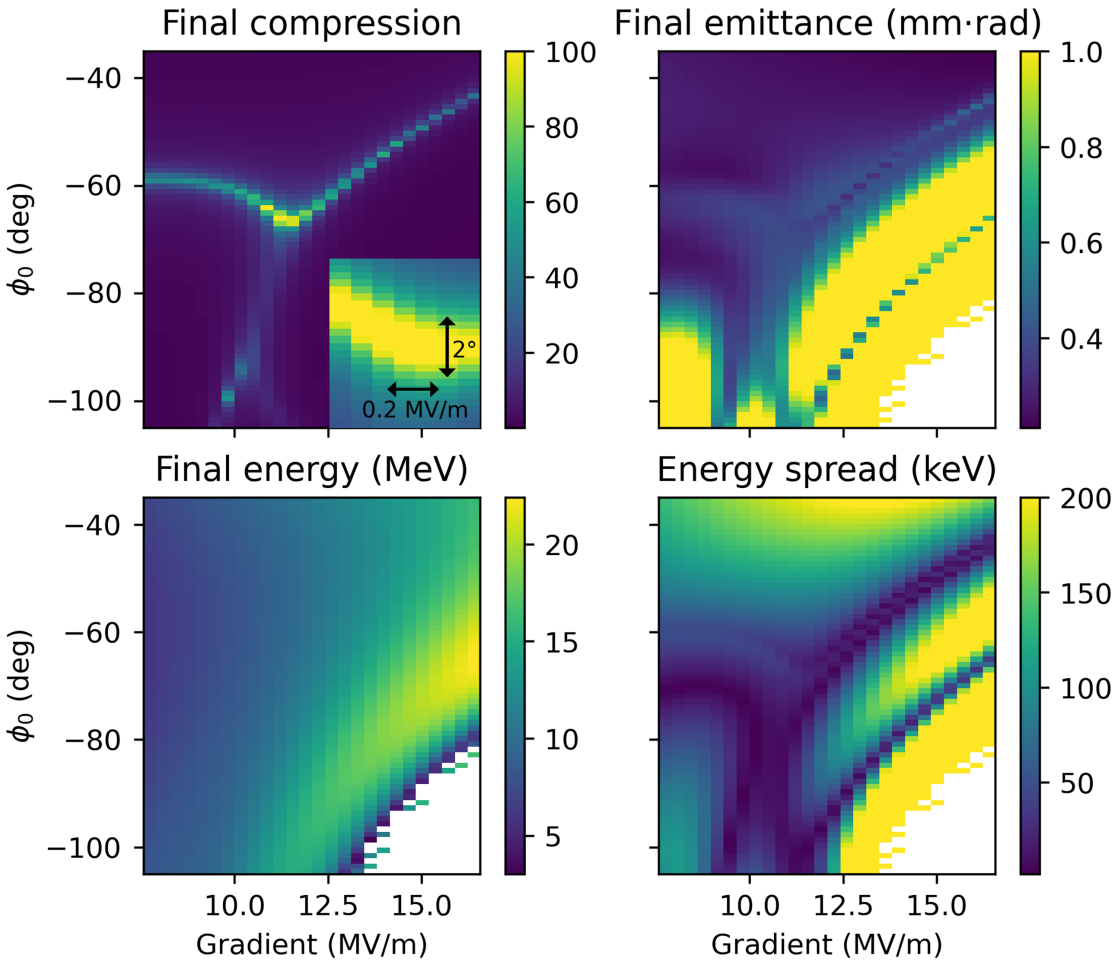

Figure 3. Scan over the cavity amplitude and phase. The plotted functions are the compression factor, bunch energy, transverse emittance and energy spread of the bunch at the exit of the TESLA cavity. The phase is measured with respect of the zero crossing of the field and the negative values of the phase correspond to the regime of deceleration.

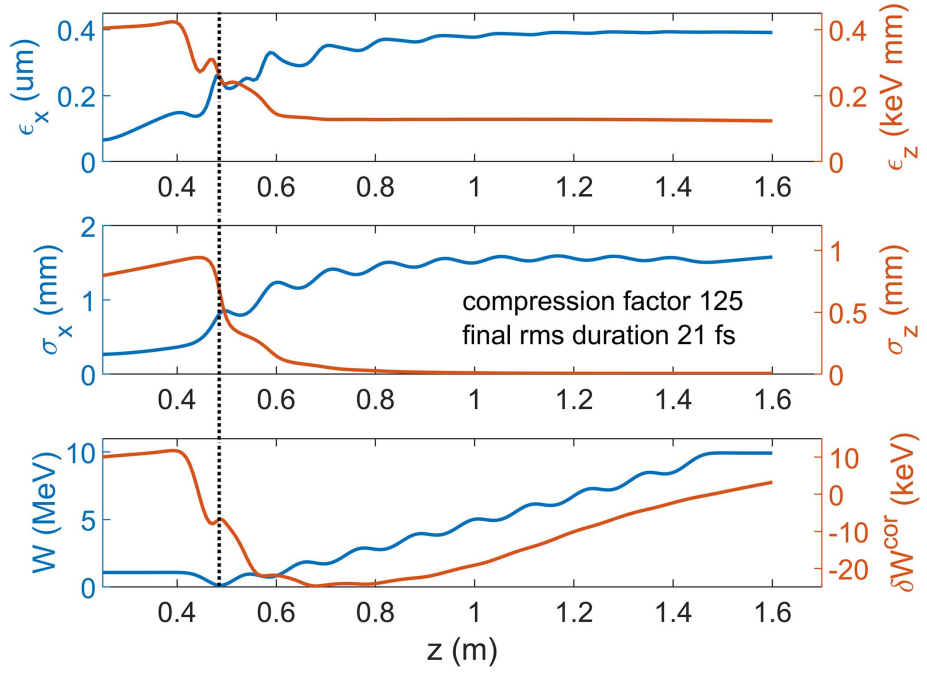

Figure 4. Evolution of the bunch parameters along the accelerating cavity: transverse and longitudinal emittances and sizes ϵ_x, ϵ_z and σ_x, σ_z; mean energy and correlated energy spread W and δW. In the simulation, $\psi_0 = -66.6^o$ and the gradient is 11 MV m^{-1}.

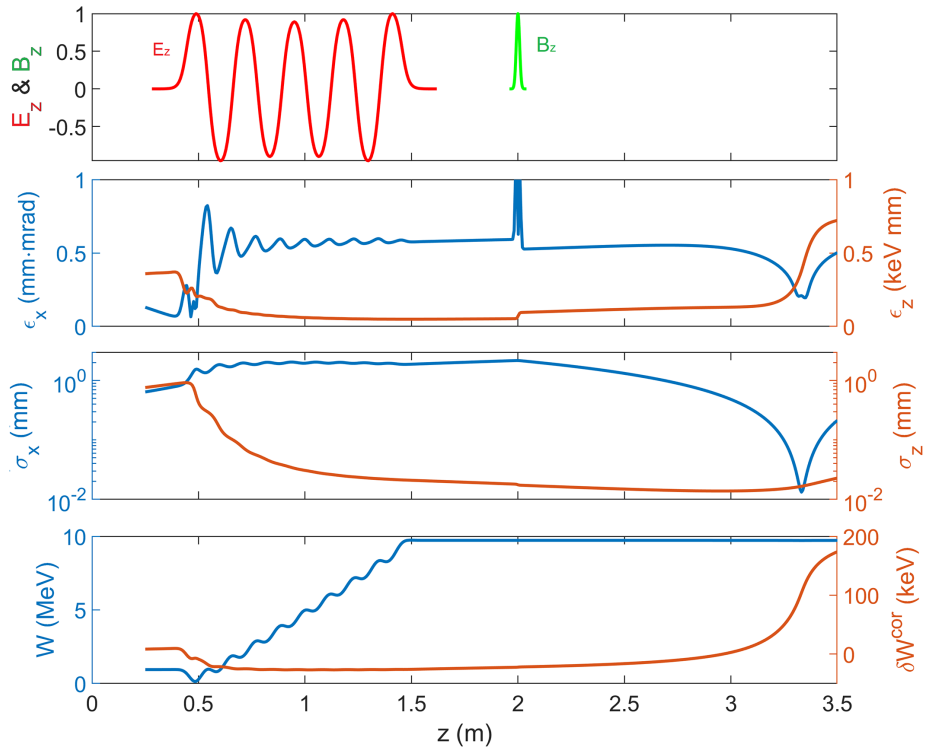

Figure 5. Evolution of the bunch parameters along an accelerator section: acceleration and longitudinal compression in a TESLA cavity, and transverse focusing by a 0.6 T solenoid. The top plot show the instantaneous electric field in the cavity normalised to unity and the magnetic field of the solenoid. In the simulation, the injection phase and gradient are -65.25^{o} and 9.7 MV m^{-1}, respectively; the beam energy at injection is 0.95 MeV.

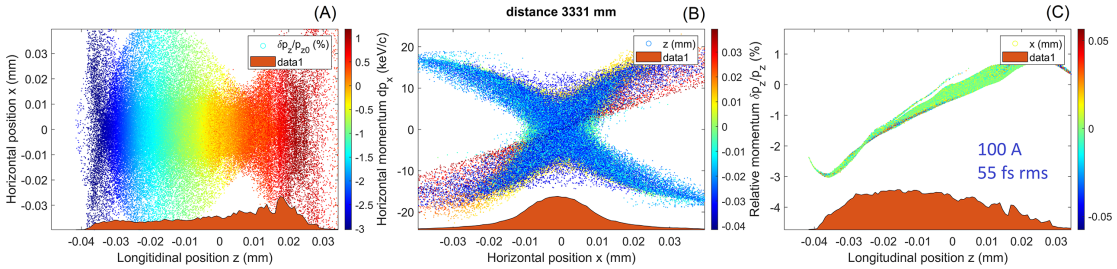

Figure 6. The plot (A) shows the distribution of electrons in the x-z plane. The relative longitudinal *momentum* of electrons is coded by the color such that the slower electrons are depicted in blue and the faster ones in red. The distribution underneath is the current density distribution along the bunch. (B) distribution of electrons in the transverse phase space (x, p_x). The relative longitudinal *position* of electrons is coded by the color such that the electrons in the tail are depicted in blue and the ones in the head in red. The distribution underneath is the projection onto the x-axis. Finally, (C) depicts the distribution of electrons in the longitudinal phase space (z, p_z). The color codes the transverse position of electrons. The distribution underneath is the projection onto the z-axis, which gives the bunch current. An animated illustration with a step of 5 mm is available in Supplementary materials.

increase substantially after 2.5 m and the longitudinal focus is reached at around 3 m. The transverse focus is reached at 3.33 m and a full graphical characterisation of the bunch in that point is shown in figure 6. At the focus the projected emittance is 0.22 mm·mrad and the mean slice emittance is 0.125 mm·mrad. The mean slice emittance can be made even smaller with another setting of the solenoid field. For a curious reader, an animated evolution of the phase space is available in Supplementary materials.

The bunch duration is 55 fs at the focus, see the second plot from the bottom in figure 5, but a better result can be achieved if the emittance compensation is done at higher beam energies. We note that for a pancake bunch, an acceleration caused by the transverse space-charge force decreases with beam energy as γ^2 whereas the longitudinal acceleration is reduced by γ^3, see, for example, chap 5 in [32, 33]. In other words, the longitudinal dynamics in the bunch caused by the space-charge force is γ 'slower' than the transverse dynamics caused by this field. This implies that in the space-charge dominated regime, the longitudinal

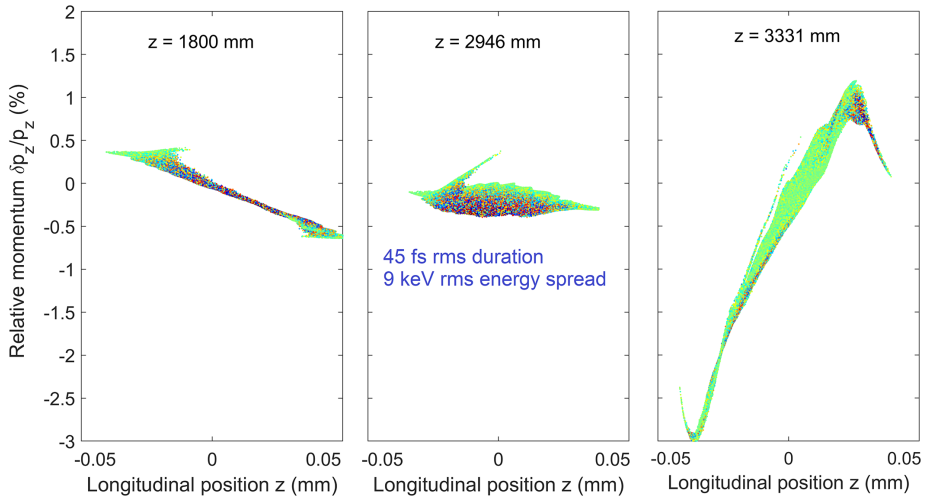

Figure 7. Longitudinal phase space of the bunch at the exit of the accelerating cavity (left plot), at the position of the maximum compression (middle) and at the position of the transverse focus (right).

depth-of-focus is roughly γ longer than the transverse one, and at sufficiently high energies it is possible to focus tightly the bunch in the transverse direction while maintaining its short duration.

In the schemes of ballistic bunching or magnetic bunching with a chicane, a nonlinear deformation of the longitudinal phase space limits bunch compression. This limitation is naturally solved in the proposed method of HWB: in the decelerating injection phase, the bunch acquires a strong convex chirp, which compensates a concave chirp acquired during further acceleration. Appreciate the linearity of the longitudinal phases-space at the exit of the accelerating cavity see the left plot in figure 7, which leads to strong compression, see the middle plot. A very low energy spread at the point of the maximum compression is the result of transfer of kinetic energy of the electrons to the potential energy of the space-charge field [18]. At the entrance to the accelerating cavity the energy spread is 8.4 keV, right after the cavity it is 25 keV, and the point of the maximum longitudinal compression the rms energy spread is reduced to 9.4 keV.

4. Low-charge regime for UED applications

The combination of ultrastrong compression and simultaneous acceleration is advantageous for UED applications with MeV electron bunches. In figure 8 the regime of compression of 16 fC electron bunches (10^5 particles) is demonstrated. A 3-cell 1.3 GHz cavity with a gradient of 7.4 MV m^{-1} is used for compression. While most of the bunch parameters are similar to those of the SLAC UED, the bunch duration of 1.2 fs rms is reached with the proposed bunching scheme whereas the bunch duration at the SLAC UED is 150 fs [10]. Detailed information about the bunch phase space is shown in figure 9. Bunch compression is limited by the 3rd order nonlinearity, which is manifested via a cubic polynomial function shape of the longitudinal phase-space distribution.

The bunch emittance is preserved during the compression, see the top plot in figure 8, thanks to a low charge so that a relatively large radius of transverse coherence of around 20 nm is achieved for a beam rms size of 0.24 mm. For comparison, via numerical simulations the compression of 80 fC bunches down to 7 fs was demonstrated by means of ballistic bunching in [34]. However, the emittance increased by a factor of 3 from 0.003 mm·mrad to 0.011 mm·mrad. The production of 0.7 fs rms bunches is also predicted in [34] using a 3rd harmonic correction cavity but the emittance grow is not discussed.

It is also instructive to compare the results of our study with those of studies [35, 36] because the latter use a conceptually similar approach: a photo-injector operated in blowout mode and a short linac operated in velocity bunching mode. The difference with our study lies in the launching (injection) phase of the injector and the use of HWB instead of the traditional velocity bunching. In [35, 36] an off-crest launching phase is used to compensate for a space-charge induced energy chirp whereas in our study no compensation is applied and the launching phase corresponds to on-crest acceleration. A comparison of the results of this study with other results in the literature is summarised in table 1. The results of the HWB systematically show either a few times better emittance or 2–3 times shorter bunch duration if the other parameters are approximately the same. Overall, electron bunch quality in the regime of HWB is well suited for ultrafast single-shot electron diffraction and x-ray generation.

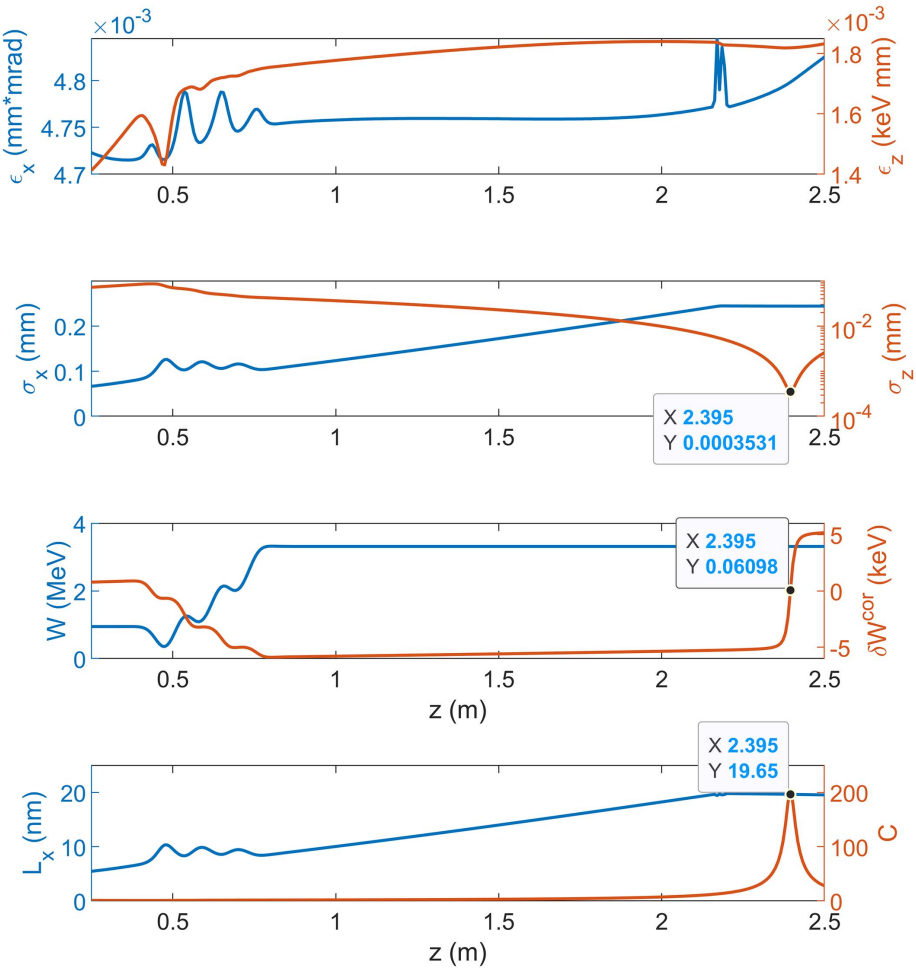

Figure 8. Evolution of the bunch parameters in a drift after exiting the accelerating cavity: transverse and longitudinal emittances and sizes ϵ_x, ϵ_z and σ_x, σ_z, respectively; mean energy and correlated energy spread W and δW; L_x is the transverse coherence radius and C is the compression factor. In the simulation, $\psi_0 = -76^o$ and the gradient 7.4 MV m^{-1}.

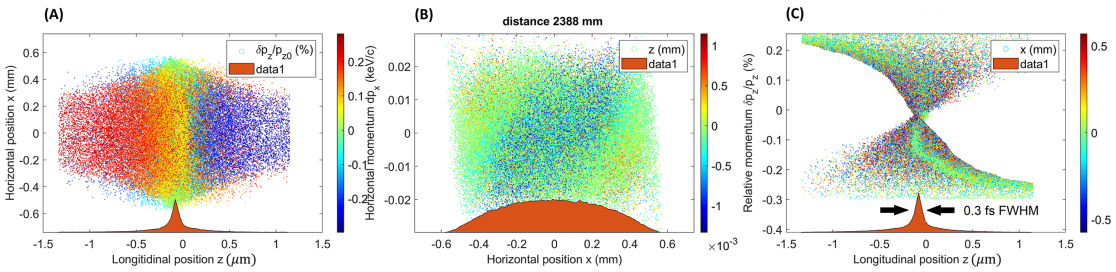

Figure 9. Phase-space distributions of a 16 fC 3.3 MeV electron bunch after compression in a 3-cell cavity.

Table 1. Comparison of the bunch parameters from several studies on the production of fs beams. The asterisk '*' is used that to indicate that the emittance data are not specified directly in the study and we estimated it from other parameters (beam size, beta function and divergence).

Parameter	This study	[36]	[37]	This study	[35]	[34]
Energy (MeV)	10	5	3.4	3.3	3.5	5
Charge (pC)	16	9	0.48	0.016	0.05	0.08
Emittance (mm·mrad)	0.22	0.5–0.6*	0.12*	0.005	0.08	0.011
Duration (fs)	55	56	15	1.2	4	7
Size (mm)	0.014	0.12	0.1	0.24	0.25	0.6

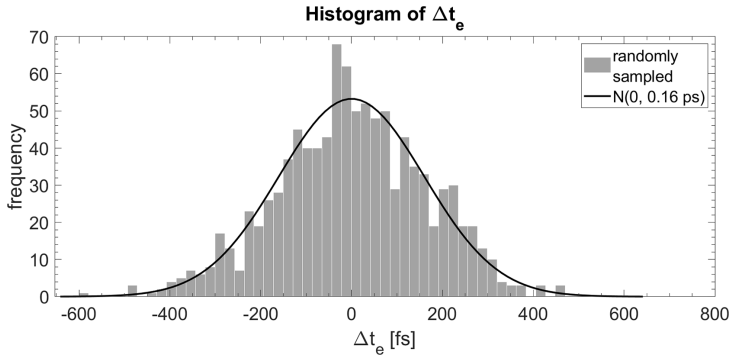

Figure 10. Histogram of randomly simulated time jitter around the optimal parameter point with probability density function normalization. The noise was Gaussian with $\sigma_{E_0} = 0.05\%$, $\sigma_\gamma = 0.05\%$, $\sigma_\phi = 0.05°$. Solid line is a Gaussian fit with parameters shown in the text.

In passing we note that the problem of time jitter can potentially be overcome by applying time stamping to the non-diffracted electrons that passed through the sample. In [37], the so-called THz oscilloscope allows determining the arrival time of electron bunches with an accuracy of 3 fs rms. Furthermore, the proposed scheme of HWB has another merit for UED applications such as a lower time jitter of a few tens of fs compared to a jitter of 180 fs in [37], see the next section.

5. Time jitter effect

To complete the analysis, we study the sensitivity of our compression scheme to a random jitter (noise) of key parameters such as the mean bunch energy, the phase and magnitude of the electric field. To investigate the dependence of bunch arrival time t_e on Gaussian jitter of parameters, we ran simulations in ASTRA with the parameters on a uniform grid around the optimal point and fitted a linear function
$\Delta t_e \approx \Delta t_{lin} = a_E \Delta E_{max} + a_\gamma \Delta\gamma + a_\phi \Delta\phi$.

The linear fit is excellent within the region of realistic deviations in the parameters, since these deviations are small. Linear maps of Gaussian variables are Gaussian and the coefficients can be used to calculate the standard deviation of the resulting Gaussian distribution for t_e: $\sigma_t^2 \approx \sigma_{t,lin}^2 = a_E^2\sigma_E^2 + a_\gamma^2\sigma_\gamma^2 + a_\phi^2\sigma_\phi^2$.

We found the following, in convenient units:

$$\sigma_t^2\ [\mathrm{fs}^2] \approx \left(\frac{1.12\,\sigma_E}{\mathrm{kVm}^{-1}}\right)^2 + \left(3.8\frac{\sigma_\gamma}{10^{-4}}\right)^2 + \left(29.6\frac{\sigma_\phi}{0.01°}\right)^2.$$

To confirm this result, we also pulled 1000 triplets of parameter noise values from independent Gaussian distributions with realistic deviations and simulated one by one to arrive at an histogram. The standard deviations used for the noise were: $\sigma_{E_0} = 0.05\%$, $\sigma_\gamma = 0.05\%$, $\sigma_\phi = 0.05°$. Figure 10 shows the results of the time jitter simulations. The time jitter indeed seems to be approximately Gaussian, with a standard deviation that agrees with the linearized calculation, 164 fs compared to 160 fs. The time jitter can be reduced down to 16 fs if the accelerator stability is pushed to the state-of-the-art regime.

To sum up, we demonstrated a novel and highly efficient regime of bunching, which allows compressing electron bunches by two orders of magnitude in a single accelerating cavity. This finding enables the production of few-fs electron beams in a very compact accelerator. Being compared to other results in the literature, see table 1, HWB systematically yields either a few times better emittance or 2–3 times shorter bunch duration if the other parameters are approximately the same. Furthermore, HWB shows resilience to RF jitter.

Data availability statement

All data that support the findings of this study are included within the article (and any supplementary files).

Acknowledgments

A O acknowledges funding through the MSCA4Ukraine Project 1232628 funded by the European Union. V G acknowledges funding from Swedish Research Council (*Vetenskapsrådet*, 2022-03983). The authors are

thankful Dr Massimo Ferrario and Dr Bas Van Der Geer for fruitful discussions. The authors also acknowledge interesting and stimulating comments from the reviewers.

Appendix. Analytical model of longitudinal compression

In the appendix we derive a useful equation for longitudinal compression in a standing wave. The electric field along the axis of a cavity, used for compression and acceleration, is given in the following general form:

$$E_z = E_0 g(z) \sin(\omega t + \varphi_0), \tag{A1}$$

where E_0 is the peak accelerating field; $g(z)$ is the normalised distribution of the electric field of the operating mode along the axis ($\max|g(z)| = 1$); ω is the angular frequency; t is the time; φ_0 is the initial (injection) RF phase at $t = 0$. The longitudinal motion of the ith particle of the bunch in the cavity field is governed by the following equations

$$\frac{d\gamma_i}{dz} = k\alpha g(z) \sin(\psi_i), \quad \frac{d\psi_i}{dz} = k\frac{\gamma_i}{\sqrt{\gamma_i^2 - 1}}, \tag{A2}$$

where $k = \omega/c$ is the wave vector in the free space; $\alpha = eE_0/kmc^2$ is the dimensionless peak accelerating field; c is the velocity of light; m is the rest mass of the electron. The longitudinal phase coordinate of the ith particle and the relativistic factor γ_i are functions of the longitudinal coordinate z and the injection time $t_{0,i}$:

$$\psi_i = \omega t(z, t_{0,i}) + \varphi_0, \quad \gamma_i = \gamma(z, t_{0,i}). \tag{A3}$$

Here $t_{0,i}$ is the initial time as the particle crosses the entrance cross-section z_0 of the cavity. The time when the particle arrives at the longitudinal coordinate z with the velocity $c\beta_z(z, t_{0,i})$ is

$$t(z, t_{0,i}) = t_{0,i} + \frac{1}{c}\int_{z_0}^{z} \frac{dz'}{\beta_z(z', t_{0,i})}. \tag{A4}$$

It is convenient to introduce the reference particle with the index r, which refers to the bunch center. Then, the longitudinal phase coordinates of the ith particle γ_i, ψ_i can be expressed through the coordinates of the reference particle γ_r, ψ_r and relative phase coordinates $\Delta\gamma_i$, $\Delta\psi_i$ as

$$\gamma_i = \gamma_r + \Delta\gamma_i, \quad \psi_i = \psi_r + \Delta\psi_i. \tag{A5}$$

Let us substitute equation (A5) into equation (A2) and taking into account the smallness of the relative phase coordinates $\Delta\psi_i \ll 1$, $\Delta\gamma_i/\gamma_r \ll 1$, Taylor expand the right hand sides in equation (A2). Restricting the expansion to linear terms, we obtain the motion equations for the relative phase coordinates

$$\frac{d\Delta\gamma_i}{dz} = k\alpha g(z) \cos(\psi_r)\Delta\psi_i, \quad \frac{d\Delta\psi_i}{dz} = -k\frac{\Delta\gamma_i}{[\gamma_r^2 - 1]^{\frac{3}{2}}}. \tag{A6}$$

Differentiating the second equation of equation (A6) with respect to z and then substituting the first one into the obtained one, we derive the equation of the pendulum with variable coefficients for the relative phase of the ith particle in the form

$$\frac{d^2\Delta\psi_i}{dz^2} + 3\gamma_r\frac{\alpha g(z)\sin(\psi_r)}{\gamma_r^2 - 1}k\frac{d\Delta\psi_i}{dz} + \frac{\alpha g(z)\cos(\psi_r)}{(\gamma_r^2 - 1)^{\frac{3}{2}}}k^2\Delta\psi_i = 0, \tag{A7}$$

where the coordinates of the reference particle γ_r, ψ_r are governed by equation (A2) with the index r.

By expanding the arrival time of the ith particle in equation (A4) with respect to the relative initial time $t_{0,i} - t_{0,r}$ in the vicinity of arrival time of the reference particle and restricting to the linear approximation, and using the definition of equation (A5), we obtain the relative phase of the ith particle in the following form

$$\Delta\psi_i = \Delta\psi_i(0)\,\eta(z), \tag{A8}$$

where $\Delta\psi_i(0) = \omega(t_{0,i} - t_{0,r})$ is the initial relative phase of the ith particle, $\eta(z)$ is the inverse bunch compression factor $C(z)$:

$$\eta(z) = C(z)^{-1} = 1 - \frac{1}{c}\int_{z_0}^{z} \frac{\left.\frac{\partial\beta_z(z',t_0)}{\partial t_0}\right|_{t_0=t_{0,r}} dz'}{\left[\beta_z(z',t_{0,r})\right]^2}. \tag{A9}$$

By substituting equation (A8) into equation (A7), we obtain an equation of longitudinal compression in the final form:

$$\frac{d^2\eta(z)}{dz^2} + 3\gamma_r\frac{\alpha g(z)\sin(\psi_r)}{{\gamma_r}^2 - 1}k\frac{d\eta(z)}{dz} + \frac{\alpha g(z)\cos(\psi_r)}{({\gamma_r}^2 - 1)^{\frac{3}{2}}}k^2\eta(z) = 0. \tag{A10}$$

From equation (A9), the initial conditions correspond to

$$\eta(z_0) = 1 \quad \text{and} \quad \eta(z_0)' = -\frac{1}{c\beta_0^2}\frac{\partial\beta_0}{\partial t_0} \tag{A11}$$

Th equation (A10) is a useful tool that allows quickly and accurately compare different regimes of bunching without time-consuming particle tracking. By multiplying equation (A10) by k^{-2} one obtains equation (2) after the substitution $\zeta = kz$.

In the linear approximation, the rms bunch phase length can be expressed through $\eta(z)$ as

$$\sigma_\psi(z) \equiv \sqrt{\langle\Delta\psi_i^2\rangle} = \sigma_\psi(0)\,|\eta(z)| \tag{A12}$$

where $\langle f_i\rangle = \frac{1}{N}\sum_{i=1}^{N} f_i$ is the operator of averaging.

References

[1] Bazarov I V, Dunham B M and Sinclair C K 2009 *Phys. Rev. Lett.* **102** 104801
[2] Sciaini G and Miller R J D 2011 *Rep. Prog. Phys.* **74** 096101
[3] Miller R J D 2014 *Annu. Rev. Phys. Chem.* **65** 583
[4] Emma P *et al* 2010 *Nat. Photon.* **4** 641
[5] Ferrario M, Clendenin J E, Palmer D T, Rosenzweig J B and Serafini L 2000 *The Physics of High Brightness Beams* (World Scientific)
[6] Hastings J B, Rudakov F M, Dowell D H, Schmerge J F, Cardoza J D, Castro J M, Gierman S M, Loos H and Weber P M 2006 *Appl. Phys. Lett.* **89** 184109
[7] Murooka Y, Naruse N, Sakakihara S, Ishimaru M, Yang J and Tanimura K 2011 *Appl. Phys. Lett.* **98** 251903
[8] Chatelain R P, Morrison V R, Godbout C and Siwick B J 2012 *Appl. Phys. Lett.* **101** 081901
[9] Giret Y, Naruse N, Daraszewicz S L, Murooka Y, Yang J, Duffy D M, Shluger A L and Tanimura K 2013 *Appl. Phys. Lett.* **103** 253107
[10] Weathersby S P *et al* 2015 *Rev. Sci. Instrum.* **86** 073702
[11] Filippetto D, Musumeci P, Li R, Siwick B, Otto M, Centurion M and Nunes J 2022 *Rev. Mod. Phys.* **94** 045004
[12] Wang X, Wu Z and Ihee H 2003 *Proc. 2003 Particle Accelerator Conf.* (*PAC-03*) (IEEE)
[13] Li R, Tang C, Du Y, Huang W, Du Q, Shi J, Yan L and Wang X 2009 *Rev. Sci. Instrum.* **80** 083303
[14] Zhu P *et al* 2015 *New J. Phys.* **17** 063004
[15] Webster D L 1939 *J. Appl. Phys.* **10** 501
[16] Lemery F and Piot P 2014 *Phys. Rev. ST Accel. Beams* **17** 112804
[17] Luiten O J, van der Geer S B, de Loos M J, Kiewiet F B and van der Wiel M J 2004 *Phys. Rev. Lett.* **93** 094802
[18] van der Geer S B, de Loos M J, van Oudheusden T, op't Root W P E M, van der Wiel M J and Luiten O J 2006 *Phys. Rev. ST Accel. Beams* **9** 044203
[19] van Oudheusden T, Pasmans P L E M, van der Geer S B, de Loos M J, van der Wiel M J and Luiten O J 2010 *Phys. Rev. Lett.* **105** 264801
[20] Anderson S G *et al* 2005 *Phys. Rev. ST Accel. Beams* **8** 014401
[21] Piot P *et al* 2004 *Proc. LINAC* pp 528–32
[22] Petrillo V, Drebot I, Ruijter M, Samsam S, Bacci A, Curatolo C, Opromolla M, Conti M R, Rossi A R and Serafini L 2023 *Appl. Sci.* **13** 752
[23] Serafini L and Ferrario M 2001 *AIP Conf. Proc.* **581** 87–106
[24] Wang X J, Qiu X and Ben-Zvi I 1996 *Phys. Rev.* E **54** R3121
[25] Piot P, Carr L, Graves W S and Loos H 2003 *Phys. Rev. ST Accel. Beams* **6** 033503
[26] Ferrario M *et al* 2010 *Phys. Rev. Lett.* **104** 054801
[27] Anderson S G *et al* 2005 *Phys. Rev. ST Accel. Beams* **8** 014401
[28] Asaka T *et al* 2017 *Phys. Rev. Accel. Beams* **20** 080702
[29] Floettmann K 1997 ASTRA - a space charge tracking algorithm (available at: www.desy.de/~mpyflo/)
[30] Shamuilov G, Opanasenko A, Pepitone K, Tibai Z and Goryashko V 2022 *New J. Phys.* **24** 123008
[31] Aune B *et al* 2000 *Phys. Rev. ST Accel. Beams* **3** 092001
[32] Reiser M 2008 *Theory and Design of Charged Particle Beams* (Wiley)
[33] Kim K-J 1989 *Nucl. Instrum. Methods Phys. Res.* A **275** 201–18
[34] Floettmann K 2014 *Nucl. Instrum. Methods Phys. Res.* A **740** 34–38
[35] Li R K, Musumeci P, Bender H A, Wilcox N S and Wu M 2011 *J. Appl. Phys.* **110** 074512
[36] Lu X, Tang C, Li R, To H, Andonian G and Musumeci P 2015 *Phys. Rev. ST Accel. Beams* **18** 032802
[37] Zhao L *et al* 2019 *Phys. Rev. Lett.* **122** 144801